TITLE OPTIONS:

1) The Electronic Properties of Atomic-Scale Strain Fields in Monolayer MoS_2

2) The effect of Atomic scale strain and strain relaxation on the electronic properties of monolayer MoS2 films
3) Local strain and strain relaxation: influence on the electronic properties of Monolayer MoS2 films

Daniel J. Trainer[1], Yuan Zhang[2], Fabrizio Bobba[1,3], Xiaoxing Xi[1], Saw-Wai Hla[2,4], Maria Iavarone[1]

[1]Physics Department, Temple University, Philadelphia PA 19122, USA

2 Center for Nanoscale Materials, Argonne National Laboratory, Argonne IL 60439

[3]Physics Department, University of Salerno, Italy

4 Physics Department, Ohio…

ABSTRACT:

The ability to control nanoscale electronic properties by introducing macroscopic strain is of critical importance for the implementation of 2D materials into flexible electronics and next generation strain engineering devices. In this work we correlate the atomic-scale lattice deformation with a systematic macroscopic bending of monolayer molybdenum disulfide films by using scanning tunneling microscopy and spectroscopy implemented with a custom-built sample holder to control the strain. Using this technique, we are able to induce strains of up to 3% before slipping effects take place and relaxation mechanisms prevail. We find a reduction of the quasiparticle band gap of about 400meV per percent local strain measured with a minimum gap of 1.2 eV. Furthermore, nanoscale strain relaxation of van der Waals monolayer sheets can negatively impact device performance. Here we investigate, for the first time, strain relaxation mechanisms including 1D ripples and 2D wrinkles which alter the spatial electronic density of states and strain distribution on the atomic-scale.

Semiconducting transition metal dichalcogenides (TMDCs), such as Molybdenum Disulfide (MoS_2), possess enormous potential for next generation nanoelectronics as a result of their relatively large band gap and 2D nature. In addition, like graphene[1], single layer MoS_2 exhibits flexibility out of plane coupled with a high intrinsic tensile strength allowing the film to sustain up to 11% strain before rupturing[2]. This intrinsic property makes this material a promising candidate for strain engineering, because it allows the application of strains high enough to considerably change the materials properties and provides therefore a large range for tuning. Thus, strain engineering offers a viable approach for applications and elects this material as prime candidate for components in future flexible devices such as mountable physiological monitoring devices, touch screens and flexible energy storage systems[3–7].

Calculations suggest that tensile strain would strongly affect the bandgap of semiconducting TMDCs[8–10], and that it would fully close at a level of biaxial tensile strain of ~10%[8,9]. Furthermore, strain is expected to change the charge carrier effective masses, dielectric properties, [11,12], thermal conductivity[13,14], spin–orbit coupling[15–17] and electrical properties [18] affecting, therefore, possible applications[19,20].

A wide range of strategies has been exploited for applying strain in nanomechanical devices incorporating 2D TMDCs. These include the use of polymer sacrificial layers[21] for the fabrication of suspended devices, transfer on a substrate with pre-patterned geometry[22], use of flexible[23–26] or piezoelectric substrates[27].

The effect of strain on the optical band gap of single layer MoS_2 and related materials has been well documented by measuring the photoluminescence spectroscopy[24,27–29], Raman spectroscopy[24,27,28,30] and absorption spectroscopy[23]. Photoluminescence measurements[23] confirmed theoretical predictions that strain could reduce the bandgap[8] and reported a change of ~70 meV per percent strain for the direct gap transition and of ~110 meV per percent strain for the indirect gap transition in bilayer MoS_2.

However, the beam diameter of such experiments, is at best a few hundred nanometers[28,29]. Thus, the effect of the applied macroscopic strain on the atomic-scale remains unclear. In addition, the quasiparticle band gap, which differs from the optical gap by the value of the exciton binding energy, has not been studied as a function of systematic strain. There is a significant difference between optical and band gap in these materials, as the exciton binding energy has been found to be large in these systems[31]. Furthermore, despite the myriad of existing literature there has not been a focus on the atomic-scale effect of a systematic strain nor a direct measurement of strain relaxation effects. Recently, Zhang et al.[32] reported on scanning tunneling microscopy measurements performed on a lateral heterojunction WSe_2-MoS_2 and revealed the local changes on the quasiparticle band gap of MoS_2. However, this study is intrinsically limited by the amount of local strain that can be applied. In this work, we report on the systematic study of the quasiparticle band gap, atomic deformation and strain relaxation effects as a function of bending radius of curvature using low temperature scanning tunneling microscopy and spectroscopy. This technique allows direct correlation between atomic scale strain and local electronic properties.

Single layer MoS_2 films are prepared by ambient pressure chemical vapor deposition on highly oriented pyrolytic graphite (HOPG). The details of the growth process can be found elsewhere[33] (see Methods). The MoS_2 films are deposited on HOPG to allow STM measurements while at the same time preventing changes of the electronic properties of MoS_2 due to the interaction with the substrate and/or avoid any possible damage of the film associated with transfer techniques. A representative atomic force microscopy (AFM) image of such a film is presented in Figure 1a, showing typical film morphologies consisting of triangular and hexagonal structures. Although, typically MoS_2 films grown on HOPG present islands of different numbers of layers, it is possible to identify the first layer of MoS_2 by STM as shown in Figure 1b. Strain is applied to the film by bending the substrate using a custom-built sample holder represented schematically in Figure 1c. This will cause a tensile strain at the substrate's surface and subsequently a strain will be transferred to the MoS_2 films until slipping mechanisms eventually

occur. The sample holder is comprised of two Cu pieces which are supported by an Omicron sample plate. The bottom piece is a semi-circular wedge which fits under the top Cu block which has a space removed with the exact dimensions of the wedge. There is a hole on the top of the block through which the STM tip can access the sample. Alignment of the tip at the top of the curvature is performed optically. The sample is placed between these two pieces and as the block is gently screwed to the sample plate it bends the sample, making it adhere to the radius of curvature of the semi-circular wedge. When a slab is bent and there is no shear relaxation on either surface, the neutral plane of the slab will maintain the same length, but the top and bottom surface will experience a tensile and compressive strain, respectively. The nominal tensile strain on the surface of the slab can be defined by the following expression:

$$\varepsilon_{Nominal} = \frac{\tau}{2R} \qquad (1)$$

Here, τ is the substrate thickness (in this case hundreds of microns) and R is the radius of curvature of the semi-circular wedge. The substrate then transfers the strain to the adhered MoS_2 film as schematically shown in Figure 1d. The STM scanner was aligned such that the fast scan direction or the X-direction, is perpendicular to the bending axis and therefore, the slow scan direction or the Y-direction is parallel to the bending axis.

Quantifying the local strain

Atomic resolution STM topographies of MoS_2 monolayer films with nominal strain of 0% and 4.9% are reported in Figures 2a and b, respectively.

To quantify the local strain, we analyze these images by using a procedure similar to the Lawler-Fujita[34] drift correction (see Supplementary Section I). This method calculates the displacement field **u**(**r**), defined as the position dependent distance between the atomic positions of the imaged lattice and a perfect periodical lattice. The derivatives of **u** along the lattice vectors directly give the strain tensor (Supplementary Section I). To obtain the average x- and y-direction

strain over an atomically resolved STM topography, $u_x(x)$ and $u_y(y)$ are plotted as a function of their respective direction. The slope of a linear fit of these curves yields the average strain. This procedure is demonstrated in Figures 2(c) and (d) which show the difference between a single layer of MoS_2 under nominal strain of 0% and maximal nominal strain, respectively. In the case of the unstrained film, the obtained strain values for the x- and y-direction are -0.12% and 0.21%. These values change to 2.67% and -1.16% for the sample with maximum nominal strain (i.e bent to a 1mm radius of curvature). MoS_2 has a positive Poisson ratio[35,36]. Since the scanner is aligned such that the x-direction, or the fast scan direction, is perpendicular to the bending axis whereas the y-direction, or the slow scan direction, is parallel to the bending axis, a tensile strain in the x-direction and a compressive strain, in the y-direction, are expected.

The average strain values in both directions have been plotted as a function of nominal strain in Figure 2e for all samples measured. The measured x-direction strain increases almost linearly until 2.5% nominal strain where the maximum local measured strain is always less than the expected nominal value. At this value of nominal strain of 2.5% we found that there are areas of the sample where there is little to no average measured strain, corresponding to a relaxed lattice. This is true to a larger extent for higher values of the nominal strain, where in the case of 4.9% the maximum local strain measured is only 3.1%. The strain in the y-direction shows a similar trend in the compressive direction. This behavior of the local strain as a function of the nominal applied strain reveals that the film is slipping with respect to the substrate, likely due to van der Waals nature of the two materials and, therefore to a weak adhesion at the interface. This slipping behavior at van der Waals interfaces has been both theoretically predicted[37] as well as experimentally reported [38] in other strain experiments.

The effect of strain on the local quasiparticle band gap

To correlate the quasiparticle density of states with local strain, tunneling spectra were acquired at multiple locations within the same atomic resolution topography images from which the local strain was obtained. These spectra were then averaged, and their quasiparticle band gap was extracted by finding the intersection point between a linear fit close to the band edge and zero conductance. Figure 3a shows representative spectra obtained at different values of nominal strain. Since, as described earlier, different areas of a sample with a given nominal strain, can have different values of local strain, the representative curves have been chosen to correspond to values of local strain closer to the nominal strain. A summary of the quasiparticle band gap extracted from the tunneling spectra plotted as a function of nominal strain and local measured strain is reported in Figures 3b and 3c, respectively. The quasiparticle band gap is found to decrease at one rate up until a nominal strain of 2.5% and at a much slower rate from 2.5% to 4.9%. Furthermore, at the nominal strain of 5% there are areas of the sample where the quasiparticle band gap resembles that of a relaxed film. These two observations are consistent with film slipping or other strain relaxation mechanisms taking place. In Figure 3c the quasiparticle band gap is plotted as a function of the local measured strain. If we focus on the positive tensile strain, a clear trend is observed, where the quasiparticle band gap reduces at a rate of approximately 400meV/% tensile strain. This rate is higher than the values reported from the optical band gap in literature[38], which fall below 100 meV/% strain. However, the effect of strain on the exciton binding energy has not been directly measured and this lacking information invalidates the exact comparison. Moreover, the optical band gap is dominated by the direct gap whereas the quasiparticle band gap, as measured by scanning tunneling spectroscopy, is an integrated average over k-space. The rate of change in the bandgap found here are much closer to those reported by Zhang et al.[32], where the authors measure the band gap change of 500 meV/% strain in lateral heterostructures comprised of WSe_2-MoS_2 by STM.

It should also be noted that all the spectra reported here were acquired away from edges, grain boundaries and defects which are known to alter the local density of states. In addition, the band gap has been found to be affected by relative orientation of the MoS_2 monolayer and that of the HOPG substrate. However this effect has been measured on this system in earlier measurements to be less than 150meV[39], therefore, clearly below the observed changes reported here.

Strain Relaxation Mechanisms

The weak inter-layer coupling between the MoS_2 and HOPG makes slipping a plausible strain relaxation mechanism as MoS_2 and HOPG are both van der Waals layered materials. However, to date, the nanoscale landscape of strain relaxation has not been studied. STM allows to measure inhomogeneous strain fields at the nanoscale and their corresponding influence on the density of states. We exploit this capability to study the possible strain relaxation mechanisms responsible for the lattice relaxation observed in the previous section. Evidence of such a mechanism is shown by the two parallel ripples in Figure 4a. A zoom in on one of the two ripples is shown in Figure 4b. This structure was found on a monolayer MoS_2 film with nominal strain of 3.3%. The scan area depicted in the topography has been acquired at an angle of 25^o with the x-direction or expected tensile strain direction. Intuitively, ripples in a sheet are caused by compressive strain. However, it has been found, using molecular dynamics simulations on CVD MoS_2, that ripples can nucleate through tensile strain and subsequent relaxation[37]. The same study shows that slipping of van der Waals layers is expected above strain values of 2%, consistent with our findings. The effect of the ripples on the local electronic properties is studied by acquiring a line profile of point tunneling spectra along the dotted line in Figure 4b reported in Figure 4c. The spectra are acquired from the region between the two ripples towards the right side of the right most ripple in Figure 4a and they are shown from the bottom to top-most spectra in Figure 4c.

There is a clear outward shift of the valence band edge of about 150meV at the point corresponding to the top of the ripple causing a larger band gap away from the parallel-ripple structure and a smaller band gap inside the two ripple structure. This can be further visualized by acquiring a conductance map at the energy just below the valence band maximum (VBM) at -1.72 eV, to determine the extent of the valence band edge shift. The conductance map is displayed in Figure 4d and shows that the increase of states at the VBM is localized between the parallel ripples, with the ripples forming the boundaries. This unique structure presents possibilities for strain engineering conduction channels in MoS_2, and similar materials.

In order to understand the strain field associated to this topographical structure, the modified Lawler-Fujita algorithm (Supplemental Section II) has been used to calculate the strain field at each atomic position in the direction perpendicular to the ripples. To highlight variations in the strain field, the average slope of the displacement field has been subtracted to give relative values of strain. The average strain removed in the direction parallel to the ripples was naturally compressive and approximately 7.6% (Supplemental Note II). The map of the strain field in the direction perpendicular to the ripples is displayed in Figure 4e and it corresponds to the topography reported in Figure 4b. It is important to note that this map provides the relative strain after the subtraction of the 7.6% average compressive strain and therefore the absolute values of compressive strain range between 4.1% and 11.1%. Given the nature of the density of states, it was expected that the region between the two ripples would yield a higher relative tensile strain than that away from the two ripples. It is also intuitive that the region on top of the ripple would experience a compressive strain relative to the surrounding regions. While both expectations are observed, there are unexpected oscillations in strain moving away from the two ripples that are not apparent in the topography. This indicates that the strain responsible for the formation of the ripple

is not localized on top of the ripple but manifests itself as oscillations which extend at least 15nm away from the ripple.

To compare the local strain field with the local electronic properties, the relative strain (obtained after subtraction of the average strain) in the direction perpendicular to the ripple in Figure 4e is plotted in Figure 4f together with the band gap extracted from the spectra in Figure 4c. The shift of the quasiparticle band gap is approximately 150meV and occurs directly at the ripple location. The gap shift starts to occur on the side of the ripple where there is the highest relative compression then there is a kink where the strain becomes relatively more positive before again increasing on the other side of the ripple where there is again a high relative compression. There is a clear suppression of the bandgap in the region between the two ripples and at the location of the right-most ripple. However, the average strain also affects the quasiparticle band gap away from the ripple as the magnitude of the band gap is reduced compared to that of the relaxed film. The changes in band gap found in the presence of large compressive strains appear to be significantly lower than those found in the presence of tensile strain (Figure 3 c). Based on DFT calculations, the compressive strain is expected to have a smaller effect on the quasiparticle band gap compared with tensile strain, consistent with our findings[40].

Other examples of relaxation mechanisms were found on monolayer MoS_2 film subjected to a nominal strain of 4.9%. Here, several regions of this film presented an inhomogeneous moiré pattern that was typically observed close to defects. This phenomenon indicates that the film undergoes a partial delamination and is well adhered to the substrate only in the regions that display the moiré pattern. An example of this kind of defect is displayed in the topography shown in Figure 5a where the film appears to be bunched around a defect with a small area showing the moiré pattern. The absolute x-direction strain map corresponding to the topography in Figure 5a

is displayed in Figure 5b. The strain map shows that there is a inhomogeneous strain field that undergoes a sharp transition from tensile strain to compressive strain on the defect and along the line where the lattice appears to be wrinkled. The area showing the moiré pattern exhibits a compressive strain compared to the surrounding area. To elucidate the electronic properties of such a defect, two line profiles of point spectra were taken perpendicular to each other. The two sequence of spectra are shown in the lower panels of Figure 5c and d, while the paths, along which the spectra were acquired, are shown in the top panels of Figure 5 c and 5d, respectively. These profiles show that there are localized in-gap states that appear directly at the defect site and that the magnitude of the gap increases, as the VBM shifts outward, in the region of the moiré pattern. To focus on the spatial variation in the electronic density of states, conductance maps were taken at a variety of different energies close to the CBM and the VBM shown in Figures 5e-j and Figures 5k-p, respectively. An increase of conductance is observed at the defect site at energy close to 1eV while a suppression of conductance is observed at around 0.7eV. Close to the VBM there are localized in-gap states at -1eV and -1.7eV that are revealed in a radius of about ½ nm surrounding the defect site. The spatial variation of the VBM displays a region of higher band gap corresponding to the less tensile strained region of the moiré pattern in topography. This appears as a low conductance region in the conductance map at energies close to the VBM around -2 eV. In this region the point spectra show an outward shift of the VBM (bottom panel of Figure 5d). Interestingly, while the variation at the conduction band edge is localized over the central defect, the variation of the valence band edge has a clear correlation with the shape of the moiré pattern in topography, where the conductance at the valence band edge shows a strong increase along the edge of the moiré pattern.

Conclusions

We have successfully applied strain on monolayer MoS_2 films of up to about 3% using a custom-built sample holder and correlated the macroscopic nominal strain with the local atomic-scale strain. Furthermore, we have correlated the local strain and the quasiparticle band gap which shows a reduction of about 400meV per percent local strain. We have observed that within the same sample, with a nominal strain of 1.5% or higher, there are regions that show local strain consistently lower than the nominal applied strain, likely due to the weak van der Waals nature of MoS_2 film and substrate. In these regions the film experiences strain relaxation that inhibited the application of strain greater than 3% using this method. Relaxation mechanisms that have been observed include formation of one dimensional ripples and two dimensional wrinkles that alter the local electronic density of states. Tunneling spectroscopy show a reduction of the band gap at the ripple location with perturbation of the local density of states that extends to a distance of 15 nm away from the ripple. Two-dimensional wrinkles found on samples with higher nominal strain, are characterized by areas displaying moiré patterns surrounding or near various defects. This suggest that the film has a nonuniform adhesion with the substrate. This nonuniform adhesion allows for the delaminating and slipping of the film with respect to the substrate and allows the formation of two-dimensional wrinkles that alter the local electronic properties of the film. These processes illustrate the weak coupling between the van der Waals layers between film and substrate and show that imposing strain of up to 3% is possible using heterostructures of this kind.

It is also important to note that locations found to have a compressive strain seem to affect less the quasiparticle band gap. Lu, et. al. [40] used DFT to investigate positive and negative strain on monolayer MoS_2 finding that not only is the band gap smaller for positive strain than it is for its negative counterpart, but that the band gap initially increases with negative strain before reducing again. This is explained to be primarily a result of the change in length of the Mo-S bond which is naturally smaller for compressive strains than for tensile strains. In the same study they also find that there is not a significant difference between uniaxial and isotropic strain in terms of

their effect on the band gap of monolayer MoS_2. This indicates that for our study, the relative orientation between the crystallographic axis and the bending axis has little influence on how the strain effects the quasiparticle band gap.

Methods

Film Growth. Single layer MoS_2 films were grown on highly pyrolytic graphite (HOPG) substrates using the ambient pressure chemical vapor deposition technique described previously[33]. The precursors used in the deposition were ~12mg of MoO_3 (≥99.5% Sigma Aldrich) and ~100mg of S powder (≥99.5% Sigma Aldrich). Otherwise the set up and heating steps were identical to those previously described [33].

STM/STS. Scanning tunneling microscopy and spectroscopy measurements were carried out using a Unisoku STM with PtIr tip at Temple University for the measurement in Figure 1b and a Createc STM with a W tip at the Center for Nanoscale Materials for the rest of the measurements. Both sets of measurements were carried out in an ultra-high vacuum ($< 10^{-10}$ Torr) at T = 4.2 K. All STM tips used in this experiment were previously prepared on Au or Ag single crystals. The STM images were recorded in constant current mode with set point parameters listed in the Figures captions. The individual dI/dV spectra found in Figure 3 were recorded by taking the numerical derivative of the measured I-V curves and applying a 10-point Savitzky-Golay smoothing. The maps and line spectroscopy in Figures 4 and 5 were obtained using a lock-in technique with a modulation voltage of 50mV and a modulation frequency of 373.1Hz.

AFM. Atomic force microscopy images were acquired in tapping mode using a Veeco Dimension Icon SPM with an Antimony (n) doped Si tip having a nominal tip radius of 10 nm (Veeco, NCHV). In this mode, the cantilever is driven to oscillate at its resonance frequency of 320 Hz by

applying an AC voltage to the z-piezo. As long as the tip is far away from the sample, no interaction is recorded and the oscillation amplitude remains constant. Once the cantilever is moved closer to the sample, the tip starts touching the surface intermittently. As a consequence, changes in the cantilever oscillation amplitude are induced by the Van der Waals interaction. In such a scenario, the amplitude modulations recorded while scanning on the surface are caused by the sample roughness. Here, a feedback loop is used to fix the tip-sample separation point-by-point in order to keep the amplitude constant. The adjustments in tip-sample distance, driven by the feedback loop, are thus a measure of sample topography. AFM measurements were carried out under ambient conditions.

REFERENCES

[1] Lee C, Wei X, Kysar J W and Hone J 2008 Measurements of the Elastic Properties and Intrinsic Strength of Monolayer Graphene *Science* **321** 385

[2] Bertolazzi S, Brivio J and Kis A 2011 Stretching and Breaking of Ultrathin MoS $_2$ *ACS Nano* **5** 9703–9

[3] Feng J, Qian X, Huang C-W and Li J 2012 Strain-engineered artificial atom as a broad-spectrum solar energy funnel *Nature Photonics* **6** 866–72

[4] Kim S J, Choi K, Lee B, Kim Y and Hong B H 2015 Materials for Flexible, Stretchable Electronics: Graphene and 2D Materials *Annual Review of Materials Research* **45** 63–84

[5] Yoon J, Park W, Bae G-Y, Kim Y, Jang H S, Hyun Y, Lim S K, Kahng Y H, Hong W-K, Lee B H and Ko H C 2013 Highly Flexible and Transparent Multilayer MoS2 Transistors with Graphene Electrodes *Small* **9** 3295–300

[6] Xu H, Wu J, Feng Q, Mao N, Wang C and Zhang J 2014 High Responsivity and Gate Tunable Graphene-MoS2 Hybrid Phototransistor *Small* **10** 2300–6

[7] Akinwande D, Petrone N and Hone J 2014 Two-dimensional flexible nanoelectronics *Nature Communications* **5**

[8] Johari P and Shenoy V B 2012 Tuning the Electronic Properties of Semiconducting Transition Metal Dichalcogenides by Applying Mechanical Strains *ACS Nano* **6** 5449–56

[9] Yue Q, Kang J, Shao Z, Zhang X, Chang S, Wang G, Qin S and Li J 2012 Mechanical and electronic properties of monolayer MoS2 under elastic strain *Physics Letters A* **376** 1166–70

[10] Shi H, Pan H, Zhang Y-W and Yakobson B I 2013 Quasiparticle band structures and optical properties of strained monolayer MoS 2 and WS 2 *Physical Review B* **87** 155304

[11] Dong L, Namburu R R, O'Regan T P, Dubey M and Dongare A M 2014 Theoretical study on strain-induced variations in electronic properties of monolayer MoS2 *Journal of Materials Science* **49** 6762–71

[12] Wang L, Kutana A and Yakobson B I 2014 Many-body and spin-orbit effects on direct-indirect band gap transition of strained monolayer MoS2 and WS2 *Annalen der Physik* **526** L7–12

[13] Kumar A and Ahluwalia P K 2013 Mechanical strain dependent electronic and dielectric properties of two-dimensional honeycomb structures of MoX2 (X=S, Se, Te) *Physica B: Condensed Matter* **419** 66–75

[14] Bhattacharyya S, Pandey T and Singh A K 2014 Effect of strain on electronic and thermoelectric properties of few layers to bulk MoS_2 *Nanotechnology* **25** 465701

[15] Rostami H, Roldán R, Cappelluti E, Asgari R and Guinea F 2015 Theory of strain in single-layer transition metal dichalcogenides *Physical Review B* **92** 195402

[16] Cheiwchanchamnangij T, Lambrecht W R L, Song Y and Dery H 2013 Strain effects on the spin-orbit-induced band structure splittings in monolayer MoS 2 and graphene *Physical Review B* **88** 155404

[17] Koskinen P, Fampiou I and Ramasubramaniam A 2014 Density-Functional Tight-Binding Simulations of Curvature-Controlled Layer Decoupling and Band-Gap Tuning in Bilayer MoS 2 *Physical Review Letters* **112** 186802

[18] Harada N, Sato S and Yokoyama N 2014 Computational study on electrical properties of transition metal dichalcogenide field-effect transistors with strained channel *Journal of Applied Physics* **115** 034505

[19] Sengupta A, Ghosh R K and Mahapatra S 2013 Performance Analysis of Strained Monolayer MoS2 MOSFET *IEEE Transactions on Electron Devices* **60** 2782–7

[20] Mohammad Tabatabaei S, Noei M, Khaliji K, Pourfath M and Fathipour M 2013 A first-principles study on the effect of biaxial strain on the ultimate performance of monolayer MoS_2 -based double gate field effect transistor *Journal of Applied Physics* **113** 163708

[21] Zhu H, Wang Y, Xiao J, Liu M, Xiong S, Wong Z J, Ye Z, Ye Y, Yin X and Zhang X 2015 Observation of piezoelectricity in free-standing monolayer MoS2 *Nature Nanotechnology* **10** 151–5

[22] Lloyd D, Liu X, Christopher J W, Cantley L, Wadehra A, Kim B L, Goldberg B B, Swan A K and Bunch J S 2016 Band Gap Engineering with Ultralarge Biaxial Strains in Suspended Monolayer MoS $_2$ *Nano Letters* **16** 5836–41

[23] He K, Poole C, Mak K F and Shan J 2013 Experimental Demonstration of Continuous Electronic Structure Tuning via Strain in Atomically Thin MoS $_2$ *Nano Letters* **13** 2931–6

[24] Zhu C R, Wang G, Liu B L, Marie X, Qiao X F, Zhang X, Wu X X, Fan H, Tan P H, Amand T and Urbaszek B 2013 Strain tuning of optical emission energy and polarization in monolayer and bilayer MoS 2 *Physical Review B* **88** 121301

[25] Conley H J, Wang B, Ziegler J I, Haglund R F, Pantelides S T and Bolotin K I 2013 Bandgap Engineering of Strained Monolayer and Bilayer MoS $_2$ *Nano Letters* **13** 3626–30

[26] Desai S B, Seol G, Kang J S, Fang H, Battaglia C, Kapadia R, Ager J W, Guo J and Javey A 2014 Strain-Induced Indirect to Direct Bandgap Transition in Multilayer WSe $_2$ *Nano Letters* **14** 4592–7

[27] Hui Y Y, Liu X, Jie W, Chan N Y, Hao J, Hsu Y-T, Li L-J, Guo W and Lau S P 2013 Exceptional Tunability of Band Energy in a Compressively Strained Trilayer MoS $_2$ Sheet *ACS Nano* **7** 7126–31

[28] Li H, Contryman A W, Qian X, Ardakani S M, Gong Y, Wang X, Weisse J M, Lee C H, Zhao J, Ajayan P M, Li J, Manoharan H C and Zheng X 2015 Optoelectronic crystal of artificial atoms in strain-textured molybdenum disulphide *Nature Communications* **6**

[29] Liu Z, Amani M, Najmaei S, Xu Q, Zou X, Zhou W, Yu T, Qiu C, Birdwell A G, Crowne F J, Vajtai R, Yakobson B I, Xia Z, Dubey M, Ajayan P M and Lou J 2014 Strain and structure heterogeneity in MoS2 atomic layers grown by chemical vapour deposition *Nature Communications* **5**

[30] Rice C, Young R J, Zan R, Bangert U, Wolverson D, Georgiou T, Jalil R and Novoselov K S 2013 Raman-scattering measurements and first-principles calculations of strain-induced phonon shifts in monolayer MoS 2 *Physical Review B* **87**

[31] Ugeda M M, Bradley A J, Shi S-F, da Jornada F H, Zhang Y, Qiu D Y, Ruan W, Mo S-K, Hussain Z, Shen Z-X, Wang F, Louie S G and Crommie M F 2014 Giant bandgap renormalization and excitonic effects in a monolayer transition metal dichalcogenide semiconductor *Nature Materials* **13** 1091–5

[32] Zhang C, Li M-Y, Tersoff J, Han Y, Su Y, Li L-J, Muller D A and Shih C-K 2018 Strain distributions and their influence on electronic structures of WSe2–MoS2 laterally strained heterojunctions *Nature Nanotechnology* **13** 152–8

[33] Trainer D J, Putilov A V, Di Giorgio C, Saari T, Wang B, Wolak M, Chandrasena R U, Lane C, Chang T-R, Jeng H-T, Lin H, Kronast F, Gray A X, Xi X, Nieminen J, Bansil A and Iavarone M 2017 Inter-Layer Coupling Induced Valence Band Edge Shift in Mono- to Few-Layer MoS2 *Scientific Reports* **7** 40559

[34] Lawler M J, Fujita K, Lee J, Schmidt A R, Kohsaka Y, Kim C K, Eisaki H, Uchida S, Davis J C, Sethna J P and Kim E-A 2010 Intra-unit-cell electronic nematicity of the high-Tc copper-oxide pseudogap states *Nature* **466** 347–51

[35] Woo S, Park H C and Son Y-W 2016 Poisson's ratio in layered two-dimensional crystals *Physical Review B* **93** 075420

[36] Woo S, Park H C and Son Y-W 2016 Erratum: Poisson's ratio in layered two-dimensional crystals [Phys. Rev. B **93** , 075420 (2016)] *Physical Review B* **94** 239901

[37] Wang J, Namburu R R, Dubey M and Dongare A M 2017 Origins of Ripples in CVD-Grown Few-layered MoS2 Structures under Applied Strain at Atomic Scales *Scientific Reports* **7** 40862

[38] Roldan R, Castellanos-Gomez A, Cappelluti E and Guinea F 2015 Strain engineering in semiconducting two-dimensional crystals *J. Phys.:Condens. Matter* **27** 313201

[39] Trainer D J, Putilov A V, Wang B, Lane C, Saari T, Chang T-R, Jeng H-T, Lin H, Xi X, Nieminen J, Bansil A and Iavarone M 2017 Moiré superlattices and 2D electronic properties of graphite/MoS 2 heterostructures *Journal of Physics and Chemistry of Solids*

[40] Lu P, Wu X, Guo W and Zeng X C 2012 Strain-dependent electronic and magnetic properties of MoS2 monolayer, bilayer, nanoribbons and nanotubes *Physical Chemistry Chemical Physics* **14** 13035

Acknowledgements. This work was supported primarily the Center for Complex Materials from First Principles (CCM), an Energy Frontier Research Center funded by the U.S. Department of Energy, Office of Science, Basic Energy Sciences under Award #SC0012575 (STM measurements, AFM measurements and thin films growth). The work at the Center for Nanoscale Materials at Argonne National Laboratory was supported by

Author Contributions. D. J. Trainer, F. Bobba and Yuan Zhang performed low temperature STM/STS measurements at the Center for Nanoscale Materials at Argonne National Laboratory under guidance of M. Iavarone and Saw Hla. D. J. Trainer fabricated MoS_2 films under guidance of X. X. Xi and he characterized the samples with AFM/STM. All authors participated in the writing of the manuscript.

Additional information

Competing financial interests: The authors declare no competing financial interests.

Author Information. Correspondence and requests for materials should be addressed to M. I. (iavarone@temple.edu).

Figures

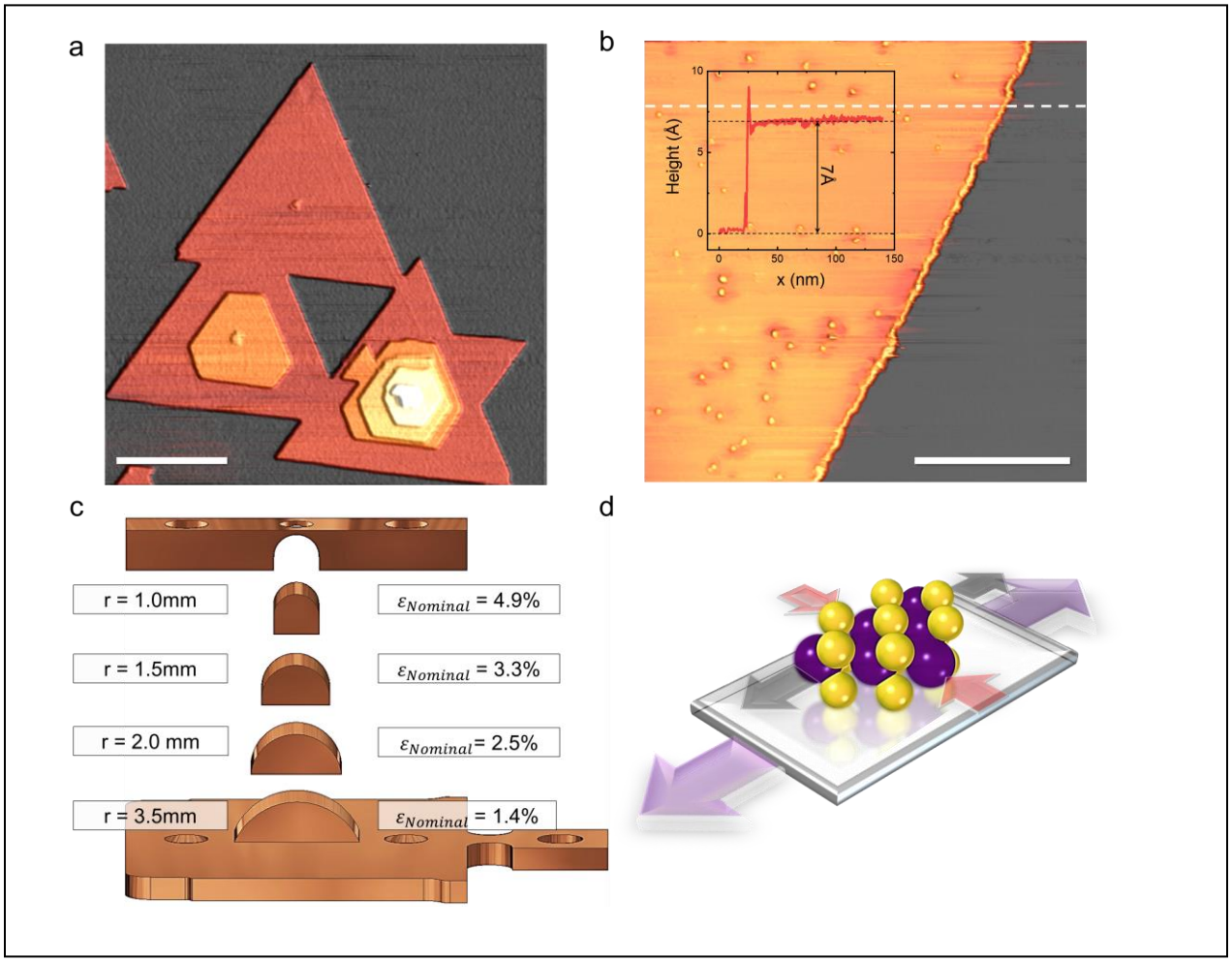

Figure 1| Strain imposing device. a, Large scale AFM topography portraying a typical morphology of the as grown CVD MoS_2 film on the graphite substrate. Scale bar represents 500nm. **b,** STM topography showing the step edge between the single layer of MoS_2 and the underlying HOPG substrate (V = -2.5 V, I = 10 pA). Scale bar represents 50nm. **c,** The custom built sample holder used to control the nominal strain on the sample. **h,** A cartoon depiction of a substrate transmitting strain to a film by bending the substrate.

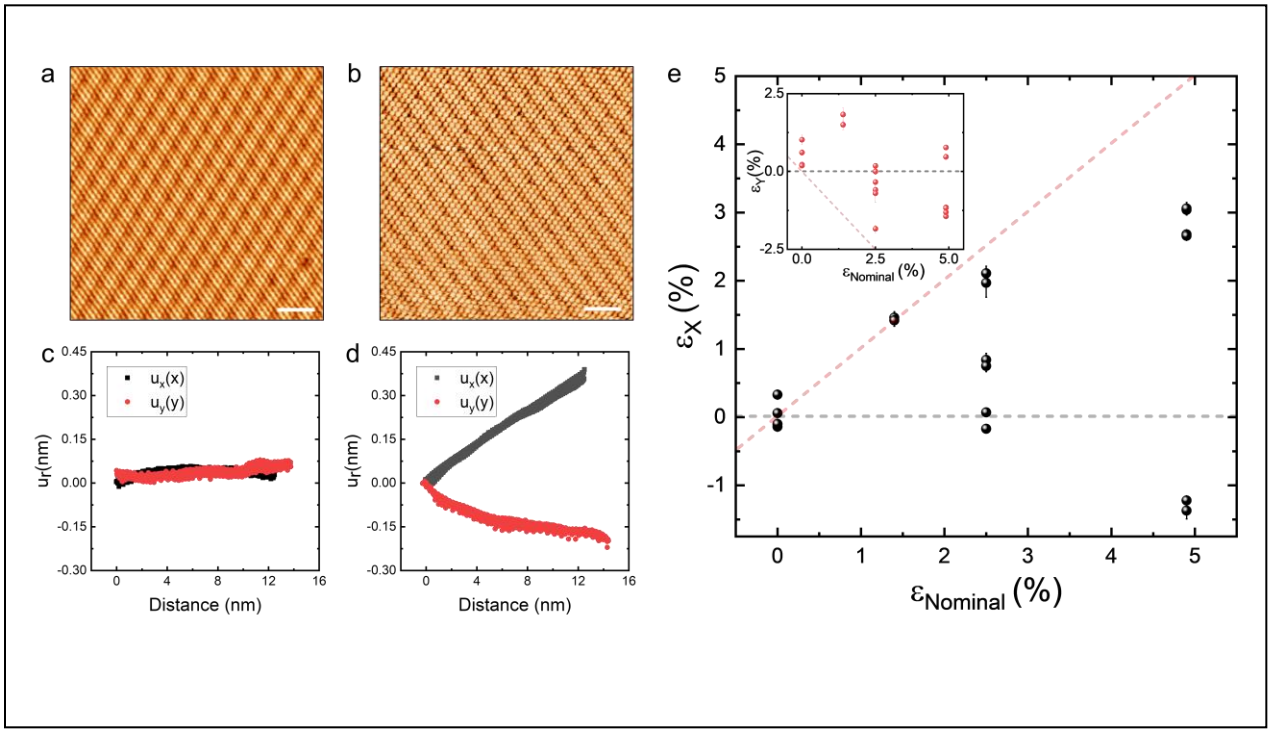

Figure 2| Atomic scale strain. a,b Atomic resolution STM topographies of single layer MoS_2 film with nominal strain of 0% (V = -1.0 V, I = 110 pA) and 4.9% **,** respectively (V = -1.5 V, I = 55 pA). Scale bars represent 2nm. **c,d** Real space determination of lattice deformation of Figure 2a **(c)** and Figure 2b **(d)**. The black squares and red circles represent the lattice distortion in the x-direction and y-direction as a function of distance in x and y, respectively. **e,** Lattice strain in the x-direction (perpendicular to the bending axis) measured as a function of nominal strain. The inset shows corresponding strain measured in the y-direction (parallel to the bending axis). The error bars represent a 95% confidence interval for the distribution of displacement field values.

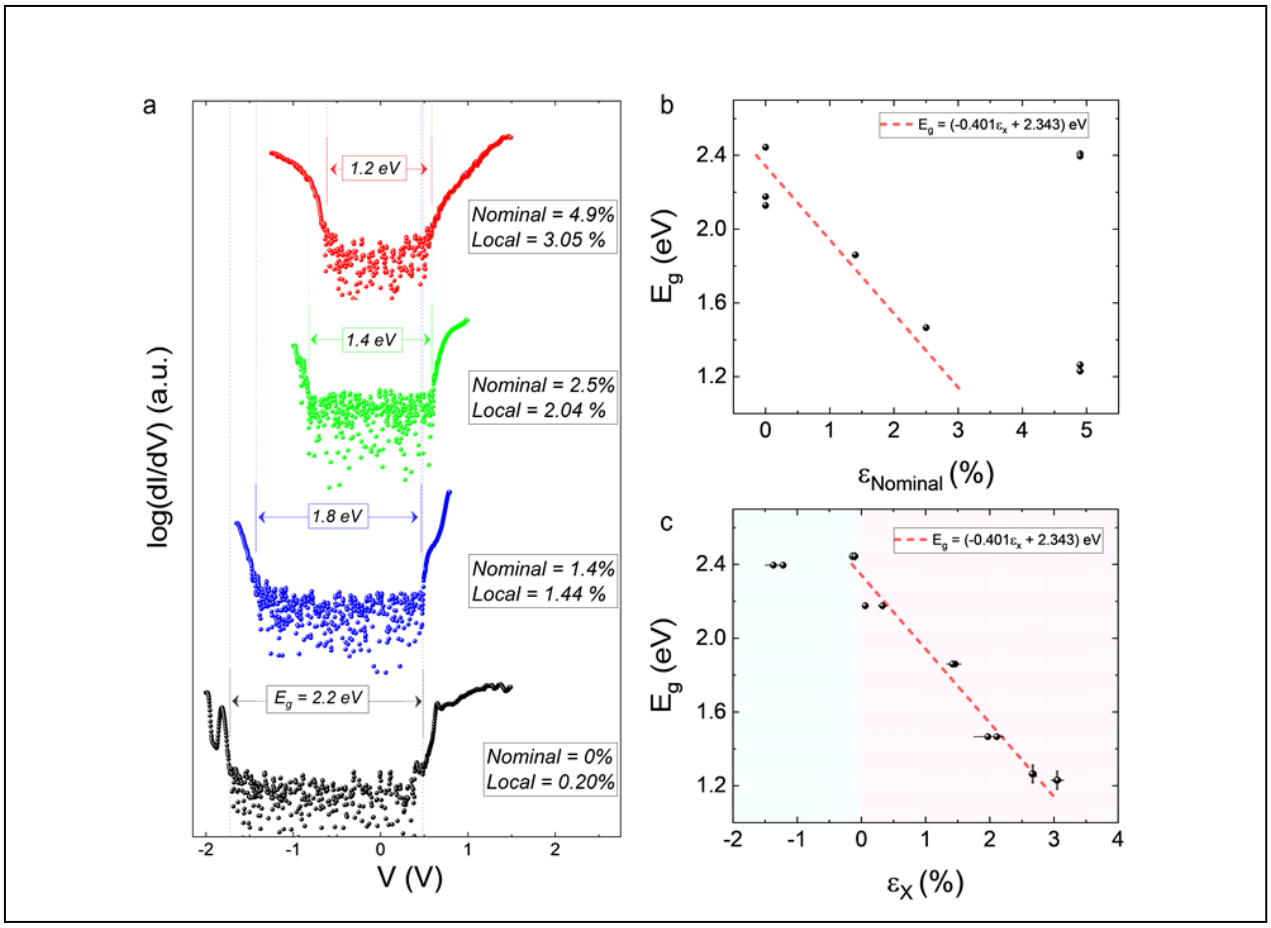

Figure 3| Effect of atomic scale strain on the quasiparticle bandgap. a, A series of vertically offset tunneling spectra taken on monolayer films displaying the minimum gap on each respective radii of curvature (V = +1.5 V or +1.0 V, I = 100 pA). **b,** A summary of the evolution of the quasiparticle band gap (E_g) as a function of the nominal strain. **c,** Corresponding summary of the evolution of the quasiparticle band gap as a function of the measured strain along the x-direction. The blue shaded region represents a compressive strain whereas the red shaded region represents a compressive strain. The dashed red line represents a linear-fit of the data displaying a compressive strain. The gap has been determined by making a linear fit to the conductance spectrum within a voltage window at the valence band and conduction band edges and finding the zero intercept. All error bars represent +/- 95% confidence interval to the mean.

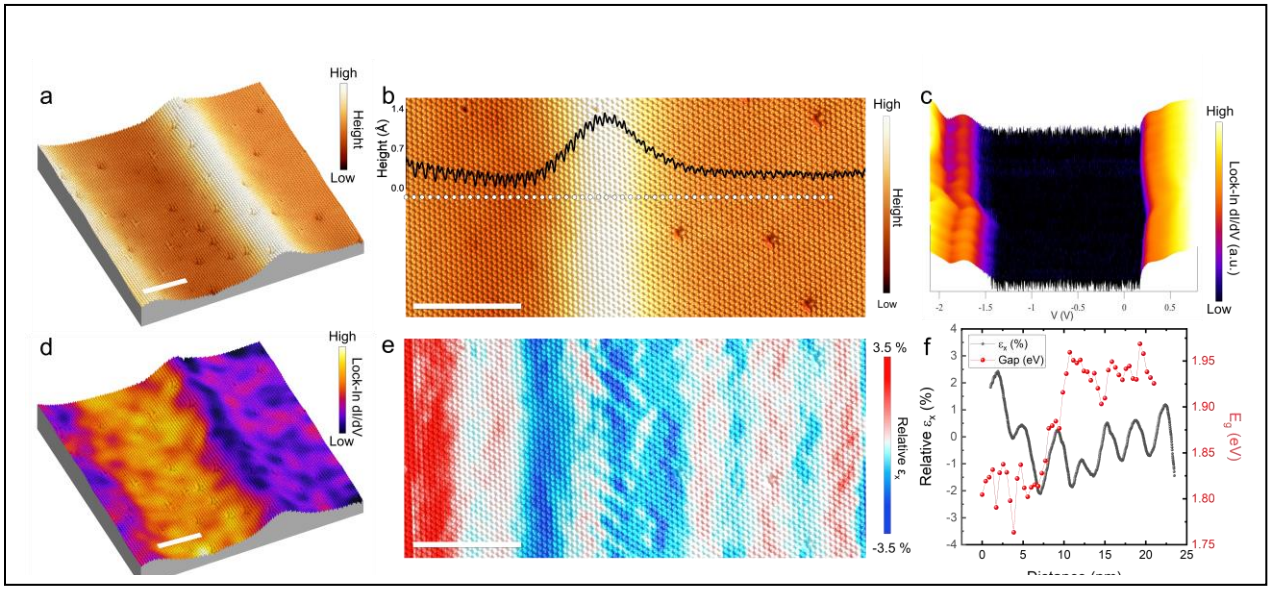

Figure 4| Electronic structure of a rippled monolayer. a, Three dimensional, high resolution STM image showing two roughly parallel ripples on monolayer MoS_2 (V = +0.8 V, I = 100 pA). **b,** An enhanced view of the ripple on the right side of Figure 4a where the region to the left of the ripple is towards the ripple on the left side of Figure 3a (V = +0.8 V, I = 100 pA). **c,** Fifty tunneling spectra displayed in log scale acquired along the dotted white line in Figure 4b where the first spectrum is taken on the left of the line (V = +1.0 V, I = 110 pA). **d,** A map of the spatial variation of the density of states in the same region as the topography in Figure 4a at an energy near the valence band edge (V = -1.72 V). **e,** A map of the spatial variation of the relative strain field in the direction perpendicular to the ripples overlaid on the 3D topography shown in Figure 4b. The average strain (slope of u_r v r) was removed to emphasize the variation in strain. **f,** The averaged relative strain across the height of Figure 4c from left to right plotted along with the quasiparticle band gap extracted from each spectrum in Figure 4c. All scale bars represent 5nm.

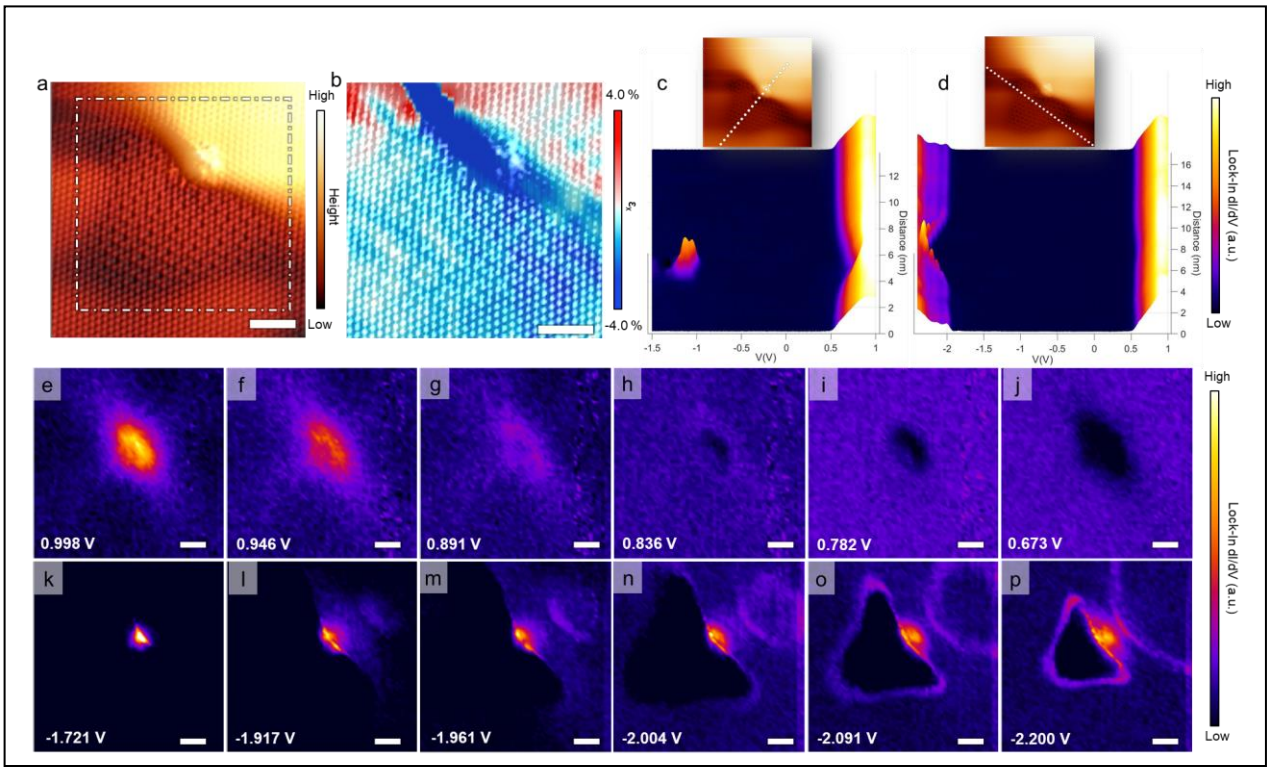

Figure 5| Spatial variation of the density of states over an inhomogeneous moiré pattern on a monolayer. a, Three dimensional, high resolution STM image showing the inhomogeneous moiré pattern at a defect site (V = -1.0V, I = 110pA). **b,** A map of the spatial variation of the relative biaxial strain field overlaid on the 3D topography from the area outlined by the dashed box in Figure 5a. The average slope (u_r vs. r) was removed to emphasize the variation in strain. All scale bars represent 2nm. **c,d** Twenty **(c)** and thirty **(d)** tunneling spectra taken over two perpendicular lines shown in their respective insets where the first spectrum is at the top right **(c)** and the top left **(d)** of the line, respectively. **e – p,** The evolution of the local density of states at energies near the conduction band edge **(e – j)** and the valence band edge **(k – p)** (V = +1.0V, I = 110pA). The voltage of the conductance map is displayed in the lower left hand corner of each figure.